SIAM J. SCI. COMPUT.
Vol. 23, No. 2, pp. 651–671

ON THREE-GRID FOURIER ANALYSIS FOR MULTIGRID*

ROMAN WIENANDS† AND CORNELIS W. OOSTERLEE†

Abstract. In this paper, we present three-grid Fourier analysis for multigrid methods. Due to the recursive structure of a multigrid iteration, this analysis can be deduced from the well-known two-grid Fourier analysis. The coarse grid correction part of multigrid algorithms can be more accurately evaluated with the three-grid analysis. We apply the analysis to several scalar equations and discretizations with an emphasis on problems with a multigrid coarse grid correction difficulty like upwind discretizations of the convection diffusion equation. The main focus lies on possible improvements by carefully chosen Galerkin operators and/or by an additional acceleration with restarted GMRES, GMRES(m). Numerical test calculations validate the theoretical predictions.

Key words. Fourier analysis, multigrid, coarse grid correction, restarted GMRES

AMS subject classifications. 65N55, 65N12, 65F10

PII. S106482750037367X

1. Introduction.

Fourier one-grid (smoothing) and two-grid analysis [2, 20, 21] are well-known tools in the multigrid community. The two-grid analysis is the basis for classical asymptotic multigrid convergence estimates [20, 21]. Moreover, it is the main analysis tool for nonsymmetric problems.

For several multigrid components or cycle variants, however, the asymptotic multigrid convergence factor cannot be predicted accurately by the Fourier two-grid factors. For example, one may use different discretizations on different grids. It can be beneficial to replace the direct $2h$-, $4h$-, etc. discretizations on the coarser grids by other discretizations. The most prominent example of this kind is the Galerkin coarse grid operator. As the entries of the Galerkin coarse grid discretizations are in general not known in advance, they may not be favorable for the smoothing method applied. Investigations of the two-grid iteration cannot display possible smoothing difficulties on coarser grids induced by the different discretizations, since the direct solution of the $2h$-problem is assumed. Furthermore, if one is interested in the influence on the asymptotic convergence factor of V-cycles versus W-cycles, of different numbers of pre- and postsmoothing, or of different smoothers on different grids, one needs to consider at least three grids.

To investigate these additional phenomena we carry out a *three*-grid Fourier analysis, which is usually sufficient to obtain a comprehensive insight into a *multi*grid method. In section 2, we outline the theoretical background of the three-grid analysis. Instead of (4×4)-blocks for the two-grid iteration matrix [2, 20, 21, 24] in the case of standard grid coarsening, the three-grid iteration matrix is transformed into a (16×16)-block matrix by Fourier analysis in the two-dimensional scalar case. This means that the calculation of three-grid asymptotic convergence factors is reduced to the calculation of the spectral radii of certain (16×16)-matrices.

In section 3, we apply the three-grid analysis to several equations and multigrid components. We focus on singular perturbation problems like the convection diffusion equation discretized by first or higher order difference schemes and the rotated

*Received by the editors June 13, 2000; accepted for publication (in revised form) November 29, 2000; published electronically July 10, 2001.
http://www.siam.org/journals/sisc/23-2/37367.html
†GMD–Institute for Algorithms and Scientific Computing (SCAI), D-53754 Saint Augustin, Germany (wienands@gmd.de, oosterlee@gmd.de).

anisotropic diffusion equation. For these problems a variety of nonstandard coarse grid discretizations is evaluated. Some of them are discussed in [26]. For example, Galerkin coarsenings based on the transfer operators from [7] and [27] are analyzed.

This analysis can be generalized to the situation where multigrid is a preconditioner for GMRES(m) [15] in the same way as it was done in [24] for the two-grid analysis. The different multigrid algorithms are not only evaluated as a solver but also as a preconditioner for GMRES(m).

2. Fourier analysis of multigrid. In this section we introduce the three-grid Fourier analysis of multigrid as a solver and as a preconditioner for GMRES(m); see sections 2.3 and 2.4, respectively. We restrict ourselves to the two-dimensional scalar case and standard coarsening, i.e., the grid coarsening is performed by doubling the mesh size in each direction, in order to keep the presentation as simple as possible. However, the generalization to three dimensions or to systems of equations is obvious but somewhat more technically involved, as explained in Remark 2. Other coarsening techniques like semicoarsening can be treated in a similar way by some appropriate changes concerning the coarse grid correction in the multigrid process.

2.1. Notation and basic principles. The rigorous theoretical foundations for the Fourier analysis of multigrid, which is also commonly called *local mode analysis*, can be found, for example, in [4] and [18]. Basically, the local mode analysis is valid if the influence of a domain boundary is negligible [4]. Often, this requirement can be fulfilled by performing some extra local relaxations near and at the boundary.

For a k-grid cycle, we consider k discrete linear operators $L_n\,(n = 1, \dots, k)$ with constant coefficients on k infinite grids G_n with mesh sizes $h_n = 2^{k-n}h$:

$$\begin{aligned} L_n u_n(\boldsymbol{x}) &= f_n(\boldsymbol{x}) \\ \text{on } \; G_n &:= \{\boldsymbol{x} = h_n \boldsymbol{j} = (h_n j_x, h_n j_y) = (x, y) \;\text{ with }\; \boldsymbol{j} \in \mathbb{Z}^2\}\,. \end{aligned} \tag{2.1}$$

Obviously, the grids become finer with an increasing index n, and L_k is defined on the finest grid with mesh size $h_k = h$. In stencil notation [20], (2.1) looks like

$$L_n u_n(\boldsymbol{x}) = \sum_{\boldsymbol{\kappa} \in J} (l_n)_{\boldsymbol{\kappa}} u_n(\boldsymbol{x} + \boldsymbol{\kappa} h_n) = f_n(\boldsymbol{x}) \;\text{ on }\; G_n \tag{2.2}$$

with stencil coefficients $(l_n)_{\boldsymbol{\kappa}}$ and a finite index set $J \subset \mathbb{Z}^2$. For compact 9-point stencils $[L]$ we have, for example,

$$J := \{\boldsymbol{\kappa} = (\kappa_x, \kappa_y) \;\text{ with }\; \kappa_x, \kappa_y \in \{-1, 0, 1\}\;\} \quad \text{and} \quad [L] = \begin{bmatrix} l_{-1,1} & l_{0,1} & l_{1,1} \\ l_{-1,0} & l_{0,0} & l_{1,0} \\ l_{-1,-1} & l_{0,-1} & l_{1,-1} \end{bmatrix}.$$

From (2.2), it can be deduced that the continuous eigenfunctions, the *Fourier components*, of the fine grid operator L_k are given by

$$\phi(\boldsymbol{\theta}, \boldsymbol{x}) := e^{i\boldsymbol{x}\boldsymbol{\theta}/h} = e^{i\boldsymbol{j}\boldsymbol{\theta}} = e^{i(j_x\theta_x + j_y\theta_y)} \;\text{ with }\; \boldsymbol{x} \in G_k\,,$$

where the *Fourier frequencies* $\boldsymbol{\theta} = (\theta_x, \theta_y)$ vary continuously in $\mathbb{R}^2$. The corresponding eigenvalues or *Fourier symbols* of L_k read as

$$\widetilde{L}_k(\boldsymbol{\theta}) = \sum_{\boldsymbol{\kappa} \in J} (l_k)_{\boldsymbol{\kappa}} e^{i\boldsymbol{\theta}\boldsymbol{\kappa}}\,. \tag{2.3}$$

On G_k, we introduce the scaled Euclidean inner product [20]

$$\langle v_k, w_k\rangle := \lim_{m\to\infty} \frac{1}{4m^2} \sum_{|\boldsymbol{\kappa}|\le m} v_k(\boldsymbol{\kappa}h)\,\overline{w_k(\boldsymbol{\kappa}h)} \quad \text{with}$$
$$|\boldsymbol{\kappa}| = \max\{|\kappa_1|, |\kappa_2|\} \quad \text{and} \quad v_k, w_k :\ G_k \longrightarrow \mathbb{C},$$

leading to a norm $||v_k|| := \sqrt{\langle v_k, v_k\rangle}$. Note that the Fourier components are orthonormal with respect to this inner product [20]. We define the space of bounded infinite grid functions by

$$\mathcal{F}(G_k) := \{v_k \mid\ v_k(\,.\,) :\ G_k \longrightarrow \mathbb{C} \ \text{ with } \ ||v_k|| < \infty\}.$$

For each $v_k \in \mathcal{F}(G_k)$, there exists a Fourier transformation, i.e., each v_k can be written as a linear combination of Fourier components [4, 11, 23]. Fourier components with $|\hat{\boldsymbol{\theta}}| := \max\{|\hat{\theta_x}|, |\hat{\theta_y}|\} \ge \pi$ are not visible on G_k, since they coincide with components $e^{i\boldsymbol{j\theta}}$, where $\boldsymbol{\theta} = \hat{\boldsymbol{\theta}} (\mathrm{mod}\, 2\pi)$, due to the periodicity of the exponential function. Therefore, the *Fourier space*

$$\mathcal{F} := \mathrm{span}\{e^{i\boldsymbol{j\theta}} : \boldsymbol{\theta} \in \Theta = (-\pi, \pi]^2\} \tag{2.4}$$

contains any bounded infinite grid-function.

It is convenient to explain the three-grid analysis (or, more generally, the k-grid analysis) by a recursive adaptation of the two-grid case. The discrete fine grid solution u_k and a current approximation u^i can be represented by linear combinations of Fourier components $e^{i\boldsymbol{j\theta}} \in \mathcal{F}$ because of $\mathcal{F}(G_k) \subset \mathcal{F}$. The same holds for the error $v^{i-1} = u^{i-1} - u_k$ before and $v^i = u^i - u_k$ after the ith k-grid cycle. It can be easily established by induction that the error transformation by a k-grid cycle is given by the following recursion [10, 20, 21]:

$$M_2^1 = S_2^{\nu_2} K_2^1 S_2^{\nu_1} = S_2^{\nu_2}(I_2 - P_1^2 (L_1)^{-1} R_2^1 L_2) S_2^{\nu_1}, \tag{2.5}$$

$$\begin{aligned} M_{\ell+2}^1 &= S_{\ell+2}^{\nu_2} K_{\ell+2}^1 S_{\ell+2}^{\nu_1} \\ &= S_{\ell+2}^{\nu_2}(I_{\ell+2} - P_{\ell+1}^{\ell+2}(I_{\ell+1} - (M_{\ell+1}^1)^\gamma)(L_{\ell+1})^{-1} R_{\ell+2}^{\ell+1} L_{\ell+2}) S_{\ell+2}^{\nu_1} \\ &\quad \text{for} \quad \ell = 1, \ldots, k-2\,, \end{aligned} \tag{2.6}$$

where the sub- and superscripts of the different operators are abbreviations for the related mesh sizes of the k involved grids. S_n is a smoothing operator on G_n, ν_1 and ν_2 indicate the number of pre- and postsmoothing iterations, K_n^1 is the coarse grid correction operator, I_n is the G_n-identity, L_n is the approximation of L_k on a coarse grid G_n, P_{n-1}^n and R_n^{n-1} are transfer operators from coarse to fine grids and reversed, and γ is the cycle index (for example, $\gamma = 1$ denotes a V-cycle and $\gamma = 2$ denotes a W-cycle). Of course, it is possible to vary the number of pre- and postsmoothing steps on the different grids leading to $\nu_1(n)$ and $\nu_2(n)$. L_{n-1} may be defined by Galerkin coarsening, $L_{n-1} = \check{R}_n^{n-1} L_n \check{P}_{n-1}^n$, or simply by a straightforward application of L_k on G_{n-1}. Note that the transfer operators in the Galerkin process do not necessarily have to match with R_n^{n-1} and P_{n-1}^n from the multigrid iteration.

For the coarse grid discretization operators, the prolongation, and the restriction, similar stencil notations as in (2.2) exist. The corresponding Fourier symbols, denoted by a tilde $\tilde{}$, are calculated as in (2.3) with a suitable index set J related to the operator under consideration; see (2.8). A detailed representation of the Fourier

symbols for many prolongations, restrictions, and discretizations is given, for instance, in [10, 20, 21, 23].

In the following, we often use a more instructive notation for the operators from (2.5), (2.6), the related Fourier symbols, and the infinite grids G_n. For example, their indices are replaced by the corresponding mesh sizes $h_n = 2^{k-n}h$. For example, we write P_{2h}^h, $\widetilde{P}_{2h}^h(\boldsymbol{\theta})$, and G_h instead of P_{k-1}^k, $\widetilde{P}_{k-1}^k(\boldsymbol{\theta})$, and G_k, respectively; see, e.g., (2.7), (2.8), or (2.11). Some basic elements of the three-grid analysis already appear in the two-grid analysis. Here, the sub- or superscript $2g$ always stands for two-grid. The index $3g$ is used accordingly for three-grid in section 2.3.

2.2. Two-grid Fourier analysis. If standard coarsening is selected, it is convenient to divide the Fourier space (2.4) into the following four-dimensional subspaces.

DEFINITION 2.1 ($2h$-harmonics). *The $2h$-harmonics $\mathcal{F}_{\boldsymbol{\theta}}^{2g}$ are given by*

$$\mathcal{F}_{\boldsymbol{\theta}}^{2g} := span\{\phi(\boldsymbol{\theta}^{\alpha_x\alpha_y}, \boldsymbol{x}) \quad with \;\; \alpha_x, \alpha_y \in \{0,1\}\;\}, \quad where$$
$$\boldsymbol{\theta} = \boldsymbol{\theta}^{00} \in \Theta_{2g} := (-\pi/2, \pi/2]^2 \quad and \;\; \boldsymbol{\theta}^{\alpha_x\alpha_y} := \boldsymbol{\theta}^{00} - (\,\alpha_x sign(\theta_x), \alpha_y sign(\theta_y)\,)\,\pi\,.$$

This distinction is motivated by the fact that each *low-frequency* $\boldsymbol{\theta}^{00} \in \Theta_{2g}$ is coupled with three *high-frequencies* $\boldsymbol{\theta}^{\boldsymbol{\alpha}}$ with $\boldsymbol{\alpha} \neq (00)$ in the transition from G_h to G_{2h}. For example, the three high-frequency components are not visible on the coarse grid as they coincide with the corresponding low-frequency component.

In order to ensure that we deal with nonsingular Fourier symbols $\widetilde{L}_h(\boldsymbol{\theta})$ and $\widetilde{L}_{2h}(2\boldsymbol{\theta})$, we restrict our considerations to the following slightly shrunken subspace of the Fourier space (2.4), as in [20]:

$$\mathcal{F}^{2g} := \mathcal{F} \setminus \bigcup_{\boldsymbol{\theta}\in\Psi_{2g}} \mathcal{F}_{\boldsymbol{\theta}}^{2g} \quad \text{with} \quad \Psi_{2g} := \{\boldsymbol{\theta} \in \Theta_{2g} :\; \widetilde{L}_{2h}(2\boldsymbol{\theta}^{00}) = 0 \;\text{ or }\; \widetilde{L}_h(\boldsymbol{\theta}^{\boldsymbol{\alpha}}) = 0\}.$$

The crucial observation is that the coarse grid correction operator K_h^{2h} (see (2.5)) leaves the spaces of $2h$-harmonics invariant for an arbitrary Fourier frequency $\boldsymbol{\theta} \in \tilde{\Theta}_{2g} := \Theta_{2g} \setminus \Psi_{2g}$. The same invariance property holds for many well-known smoothing methods, e.g., Jacobi point- or line-relaxation, lexicographical Gauss–Seidel point- or line-relaxation, and certain pattern relaxation methods such as red-black Gauss–Seidel or zebra line Gauss–Seidel. Especially for pattern relaxations, the calculation of the related Fourier symbols is not as simple as it is for the different operators of the coarse grid correction. In general, certain Fourier components within the spaces of $2h$-harmonics may be coupled by the smoothing operator, which means that the calculation of the corresponding Fourier symbol cannot be done separately for each component $\phi(\boldsymbol{\theta}, \boldsymbol{x})$, as in (2.3). On the contrary, it is represented by a general (4×4)-matrix $S^{2g}(\boldsymbol{\theta}, h) = S^{2g}(\boldsymbol{\theta}^{00}, \boldsymbol{\theta}^{11}, \boldsymbol{\theta}^{10}, \boldsymbol{\theta}^{01}, h) \in \mathbb{C}^{4\times 4}$. For the explicit representation of several relaxation methods, we refer to [10, 20, 21, 23].

Summarizing, we have that the two-grid operator (see (2.5)) leaves the spaces of $2h$-harmonics invariant, i.e., for each $\boldsymbol{\theta} \in \tilde{\Theta}_{2g}$ it holds that

$$M_h^{2h}|_{\mathcal{F}_{\boldsymbol{\theta}}^{2g}} \triangleq M^{2g}(\boldsymbol{\theta}, h) \tag{2.7}$$
$$= (S^{2g}(\boldsymbol{\theta}, h))^{\nu_2}(\, I^{2g} - P^{2g}(\boldsymbol{\theta}, h)(\mathcal{L}^{2g}(\boldsymbol{\theta}, h))^{-1} R^{2g}(\boldsymbol{\theta}, h) L^{2g}(\boldsymbol{\theta}, h)\,)(S^{2g}(\boldsymbol{\theta}, h))^{\nu_1}\,.$$

The representation of the coarse grid correction block matrices is given by

$$
\begin{aligned}
I^{2g} &= \mathrm{diag}\{1,1,1,1\} \in \mathbb{C}^{4\times 4}\,, \quad \mathcal{L}^{2g}(\boldsymbol{\theta},h) = \widetilde{L}_{2h}(2\boldsymbol{\theta}^{00}) \in \mathbb{C}^{1\times 1}\,,\\
L^{2g}(\boldsymbol{\theta},h) &= \mathrm{diag}\{\widetilde{L}_h(\boldsymbol{\theta}^{00}),\widetilde{L}_h(\boldsymbol{\theta}^{11}),\widetilde{L}_h(\boldsymbol{\theta}^{10}),\widetilde{L}_h(\boldsymbol{\theta}^{01})\} \in \mathbb{C}^{4\times 4}\,,\\
R^{2g}(\boldsymbol{\theta},h) &= (\,\widetilde{R}_h^{2h}(\boldsymbol{\theta}^{00})\,\widetilde{R}_h^{2h}(\boldsymbol{\theta}^{11})\,\widetilde{R}_h^{2h}(\boldsymbol{\theta}^{10})\,\widetilde{R}_h^{2h}(\boldsymbol{\theta}^{01})\,) \in \mathbb{C}^{1\times 4}\,,\\
P^{2g}(\boldsymbol{\theta},h) &= (\,\widetilde{P}_{2h}^{h}(\boldsymbol{\theta}^{00})\,\widetilde{P}_{2h}^{h}(\boldsymbol{\theta}^{11})\,\widetilde{P}_{2h}^{h}(\boldsymbol{\theta}^{10})\,\widetilde{P}_{2h}^{h}(\boldsymbol{\theta}^{01})\,)^T \in \mathbb{C}^{4\times 1}\,.
\end{aligned}
\tag{2.8}
$$

Using the simple block representation from (2.7), the spectral radius of the two-grid iteration matrix and thus the asymptotic two-grid convergence factor can be approximated by

$$
\rho_{2g}(h) := \sup_{\boldsymbol{\theta}\in\tilde{\Theta}_{2g}} \rho(M^{2g}(\boldsymbol{\theta},h))\,. \tag{2.9}
$$

Remark 1 (boundedness of $\rho_{2g}(h)$). In all the examples considered in section 3, we have $\tilde{\Theta}_{2g} = (-\pi/2,\pi/2]\setminus\{(0,0)\}$, as only $\widetilde{L}_h((0,0))$ and $\widetilde{L}_{2h}(2(0,0))$ are zero. However, the suprenum in (2.9) remains finite, since $\widetilde{R}_h^{2h}((0,0))\widetilde{L}_h((0,0))$ is rank deficient too, in such a way that $\lim_{\boldsymbol{\theta}\to(0,0)}\rho(M^{2g}(\boldsymbol{\theta},h))$ is bounded; see [4].

The smoothing or one-grid convergence factor $\rho_{1g}(h)$, based on the "ideal" coarse grid correction operator Q_h^{2h} with $Q_h^{2h}|_{\mathcal{F}_{\boldsymbol{\theta}}^{2g}} \triangleq Q = \mathrm{diag}\{0,1,1,1\}$ from [20], reads as

$$
\rho_{1g}(h) := \sup_{\boldsymbol{\theta}\in\tilde{\Theta}_{2g}} \rho(\,Q(S^{2g}(\boldsymbol{\theta},h))^{\nu_1+\nu_2}\,)\,. \tag{2.10}
$$

Q_h^{2h} annihilates the low-frequency error components and leaves the high-frequency components unchanged. $\rho_{1g}(h)$ yields reasonable convergence estimates as long as Q_h^{2h} is a good approximation of the real coarse grid correction operator.

2.3. Three-grid Fourier analysis. From (2.6), the error transformation by a three-grid cycle is given by $v_i = M_h^{4h} v_{i-1}$ with

$$
\begin{aligned}
M_h^{4h} &= S_h^{\nu_2} K_h^{4h} S_h^{\nu_1}\\
&= S_h^{\nu_2}(I_h - P_{2h}^h(I_{2h} - (M_{2h}^{4h})^\gamma)(L_{2h})^{-1}R_h^{2h}L_h)S_h^{\nu_1}\,,
\end{aligned}
\tag{2.11}
$$

where M_{2h}^{4h}, defined by (2.5), reads as

$$
M_{2h}^{4h} = S_{2h}^{\nu_2}(I_{2h} - P_{4h}^{2h}(L_{4h})^{-1}R_{4h}^{2h}L_{2h})S_{2h}^{\nu_1}\,. \tag{2.12}
$$

Instead of inverting L_{2h}, as is done in the two-grid cycle (2.5), the $2h$-equation is solved approximately by performing γ two-grid iterations M_{2h}^{4h} with zero initial approximation. This is reflected by the replacement of $(L_{2h})^{-1}$ from (2.5) by the expression

$$
(\mathcal{L}_{2h}^{4h})^{-1} = (I_{2h} - (M_{2h}^{4h})^\gamma)(L_{2h})^{-1} \tag{2.13}
$$

in (2.11). To see this, consider an arbitrary nonsingular system $Lu = f$ which is approximately solved by γ steps of an iterative method, $Cu^j = (C-L)u^{j-1} + f$, based on the splitting $L = C + (L-C)$. If a multigrid method is applied, we obtain $u^j = Mu^{j-1} + C^{-1}f$ with $C^{-1} = (I-M)L^{-1}$. M denotes the error transformation matrix by one multigrid cycle; see (2.6). Starting with $u^0 = 0$, the γth iterate can easily be written as $u^\gamma = (I - M^\gamma)L^{-1}f$. In a numerical algorithm, however, L^{-1} (and, in particular, $(L_{2h})^{-1}$) is, of course, not applied explicitly.

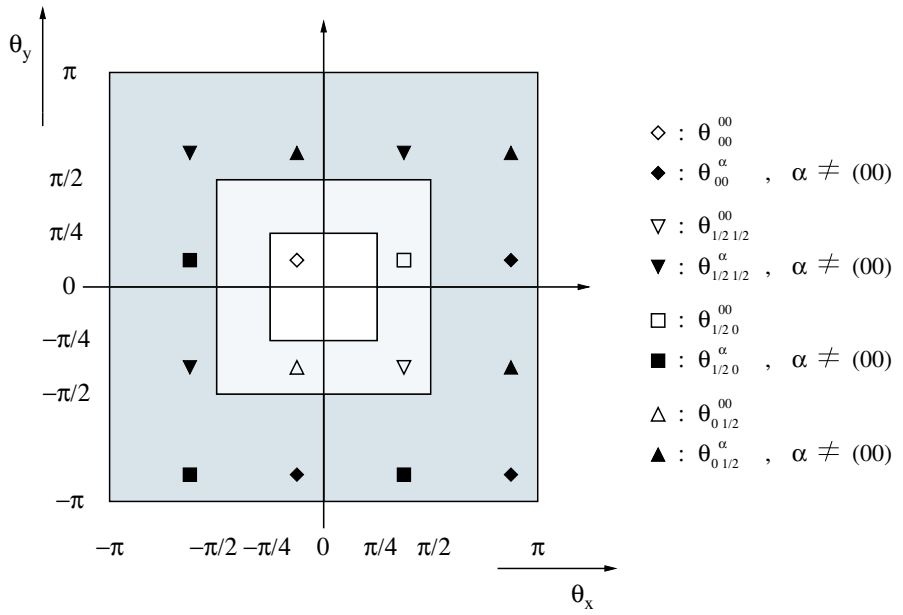

FIG. 2.1. *A set of Fourier frequencies that are coupled by a three-grid iteration; see Definition* 2.2.

Considering three-grid cycles, it is appropriate to divide the Fourier space $\mathcal{F}$ into a direct sum of the following 16-dimensional subspaces.

DEFINITION 2.2 ($4h$-harmonics). *The $4h$-harmonics are defined by*

$$\begin{aligned}\mathcal{F}^{3g}_{\boldsymbol{\theta}} := span\Big\{ & \phi(\boldsymbol{\theta}^{\boldsymbol{\alpha}}_{\boldsymbol{\beta}}, \boldsymbol{x}) \quad with \;\; \boldsymbol{\alpha} = (\alpha_x\, \alpha_y)\,, \;\; \boldsymbol{\beta} = (\beta_x\, \beta_y), \\ & \qquad and \;\; \alpha_x, \alpha_y \in \{0,1\}\,, \;\; \beta_x, \beta_y \in \Big\{0, \frac{1}{2}\Big\}\;\Big\}, \\ & where \quad \boldsymbol{\theta} = \boldsymbol{\theta}^{00}_{00} \in \Theta_{3g} := (-\pi/4, \pi/4]^2 \quad and \\ & \boldsymbol{\theta}^{00}_{\beta_x\beta_y} = \boldsymbol{\theta}^{00}_{00} - (\,\beta_x sign(\theta_x), \beta_y sign(\theta_y)\,)\pi\,, \\ & \boldsymbol{\theta}^{\alpha_x\alpha_y}_{\boldsymbol{\beta}} = \boldsymbol{\theta}^{00}_{\boldsymbol{\beta}} - (\,\alpha_x sign(\theta_{\beta_x}), \alpha_y sign(\theta_{\beta_y})\,)\pi\,.\end{aligned}$$

Figure 2.1 illustrates this somewhat technical definition by indicating the location of the 16 different frequencies $\boldsymbol{\theta}^{\boldsymbol{\alpha}}_{\boldsymbol{\beta}}$. It can be motivated in the same way as it was done in the two-grid analysis concerning the $2h$-harmonics. In the transition from G_{2h} to G_{4h}, a low frequency $\boldsymbol{\theta}^{00}_{00} \in \Theta_{3g}$ is coupled with three high frequencies $\boldsymbol{\theta}^{00}_{\boldsymbol{\beta}}$ with $\boldsymbol{\beta} \neq (00)$. We collect four such components in the following subspaces.

DEFINITION 2.3.

$$\mathcal{F}^{\boldsymbol{\beta}}_{\boldsymbol{\theta}} := span\Big\{\phi(\boldsymbol{\theta}^{00}_{\beta_x\beta_y}, \boldsymbol{x}) \quad with \;\; \beta_x, \beta_y \in \Big\{0, \frac{1}{2}\Big\}\;\Big\} \quad for \;\; \boldsymbol{\theta}^{00}_{00} \in \Theta_{3g}\,.$$

Furthermore, each $\boldsymbol{\theta}^{00}_{\boldsymbol{\beta}}$ is coupled with three high-frequency components $\boldsymbol{\theta}^{\boldsymbol{\alpha}}_{\boldsymbol{\beta}}$ with $\boldsymbol{\alpha} \neq (00)$ in the transition from G_h to G_{2h}; see Figure 2.1. It follows that a three-grid cycle couples 16 frequencies, i.e., the 15 high-frequency components alias on G_{4h} with the low-frequency component $\phi(\boldsymbol{\theta}^{00}_{00}, \boldsymbol{x})$.

Again, we exclude certain frequencies from the calculation to obtain a well-defined three-grid operator and consider the following slightly smaller spaces:

$$\mathcal{F}^{3g} := \mathcal{F} \setminus \bigcup_{\boldsymbol{\theta}\in\Psi_{3g}} \mathcal{F}^{3g}_{\boldsymbol{\theta}} \quad \text{and} \quad \tilde{\Theta}_{3g} := \Theta_{3g} \setminus \Psi_{3g} \quad \text{with}$$
$$\Psi_{3g} := \left\{ \boldsymbol{\theta} \in \Theta_{3g} : \ \widetilde{L}_{4h}(4\boldsymbol{\theta}^{00}_{00}) = 0 \ \text{ or } \ \widetilde{L}_{2h}(2\boldsymbol{\theta}^{00}_{\boldsymbol{\beta}}) = 0 \ \text{ or } \ \widetilde{L}_{h}(\boldsymbol{\theta}^{\boldsymbol{\alpha}}_{\boldsymbol{\beta}}) = 0 \right\}.$$

Comparing Definitions 2.1 and 2.2, it immediately follows that each space of $4h$-harmonics consists of four spaces of $2h$-harmonics, i.e., for an arbitrary $\boldsymbol{\theta} \in \tilde{\Theta}_{3g}$ we have

$$\mathcal{F}^{3g}_{\boldsymbol{\theta}} = \mathcal{F}^{2g}_{\boldsymbol{\theta}^{00}_{00}} \cup \mathcal{F}^{2g}_{\boldsymbol{\theta}^{00}_{\frac{1}{2}\frac{1}{2}}} \cup \mathcal{F}^{2g}_{\boldsymbol{\theta}^{00}_{\frac{1}{2}0}} \cup \mathcal{F}^{2g}_{\boldsymbol{\theta}^{00}_{0\frac{1}{2}}} . \tag{2.14}$$

As a fundamental statement for the three-grid analysis, we find that the three-grid operator M^{4h}_h (2.11) leaves the spaces of $4h$-harmonics invariant. Using Definition 2.3, (2.14), and the considerations from the last subsection, it follows for every $\boldsymbol{\theta} \in \tilde{\Theta}_{3g}$ that

$$\begin{aligned} &S_h : \mathcal{F}^{3g}_{\boldsymbol{\theta}} \longrightarrow \mathcal{F}^{3g}_{\boldsymbol{\theta}}, \quad L_h : \mathcal{F}^{3g}_{\boldsymbol{\theta}} \longrightarrow \mathcal{F}^{3g}_{\boldsymbol{\theta}}, \\ &R^{2h}_h : \mathcal{F}^{3g}_{\boldsymbol{\theta}} \longrightarrow \mathcal{F}^{\boldsymbol{\beta}}_{\boldsymbol{\theta}}, \quad \mathcal{L}^{4h}_{2h} : \mathcal{F}^{\boldsymbol{\beta}}_{\boldsymbol{\theta}} \longrightarrow \mathcal{F}^{\boldsymbol{\beta}}_{\boldsymbol{\theta}}, \quad P^{h}_{2h} : \mathcal{F}^{\boldsymbol{\beta}}_{\boldsymbol{\theta}} \longrightarrow \mathcal{F}^{3g}_{\boldsymbol{\theta}} . \end{aligned} \tag{2.15}$$

The relation for $\mathcal{L}^{4h}_{2h}$ reads in more detail as (see (2.13) and (2.12))

$$\begin{aligned} &L_{2h} : \mathcal{F}^{\boldsymbol{\beta}}_{\boldsymbol{\theta}} \longrightarrow \mathcal{F}^{\boldsymbol{\beta}}_{\boldsymbol{\theta}}, \quad S_{2h} : \mathcal{F}^{\boldsymbol{\beta}}_{\boldsymbol{\theta}} \longrightarrow \mathcal{F}^{\boldsymbol{\beta}}_{\boldsymbol{\theta}}, \quad R^{4h}_{2h} : \mathcal{F}^{\boldsymbol{\beta}}_{\boldsymbol{\theta}} \longrightarrow \operatorname{span}\{\phi(\boldsymbol{\theta}^{00}_{00}, \boldsymbol{x})\}, \\ &L_{4h} : \operatorname{span}\{\phi(\boldsymbol{\theta}^{00}_{00}, \boldsymbol{x})\} \longrightarrow \operatorname{span}\{\phi(\boldsymbol{\theta}^{00}_{00}, \boldsymbol{x})\}, \quad P^{2h}_{4h} : \operatorname{span}\{\phi(\boldsymbol{\theta}^{00}_{00}, \boldsymbol{x})\} \longrightarrow \mathcal{F}^{\boldsymbol{\beta}}_{\boldsymbol{\theta}} . \end{aligned}$$

As a consequence of (2.15), one obtains the following (16×16)-block matrices:

$$\begin{aligned} M^{4h}_h|_{\mathcal{F}^{3g}_{\boldsymbol{\theta}}} &\stackrel{\wedge}{=} M^{3g}(\boldsymbol{\theta}, h) \\ &= (S^{3g}(\boldsymbol{\theta}, h))^{\nu_2} (I^{3g} - P^{3g}(\boldsymbol{\theta}, h)(\mathcal{L}^{3g}(\boldsymbol{\theta}, h))^{-1} R^{3g}(\boldsymbol{\theta}, h) L^{3g}(\boldsymbol{\theta}, h)) (S^{3g}(\boldsymbol{\theta}, h))^{\nu_1} . \end{aligned} \tag{2.16}$$

The different operators of the block-matrices $M^{3g}(\boldsymbol{\theta}, h)$ can be expressed by the two-grid representations from section 2.2; see $S^{2g}(\boldsymbol{\theta}, h)$ and (2.8):

$$\begin{aligned} I^{3g} &= \operatorname{diag}\{I^{2g}, I^{2g}, I^{2g}, I^{2g}\} \in \mathbb{C}^{16\times 16}, \\ S^{3g}(\boldsymbol{\theta}, h) &= \operatorname{diag}\{S^{2g}(\boldsymbol{\theta}_{00}, h), S^{2g}(\boldsymbol{\theta}_{\frac{1}{2}\frac{1}{2}}, h), S^{2g}(\boldsymbol{\theta}_{\frac{1}{2}0}, h), S^{2g}(\boldsymbol{\theta}_{0\frac{1}{2}}, h)\} \in \mathbb{C}^{16\times 16}, \\ L^{3g}(\boldsymbol{\theta}, h) &= \operatorname{diag}\{L^{2g}(\boldsymbol{\theta}_{00}, h), L^{2g}(\boldsymbol{\theta}_{\frac{1}{2}\frac{1}{2}}, h), L^{2g}(\boldsymbol{\theta}_{\frac{1}{2}0}, h), L^{2g}(\boldsymbol{\theta}_{0\frac{1}{2}}, h)\} \in \mathbb{C}^{16\times 16}, \\ R^{3g}(\boldsymbol{\theta}, h) &= \operatorname{diag}\{R^{2g}(\boldsymbol{\theta}_{00}, h), R^{2g}(\boldsymbol{\theta}_{\frac{1}{2}\frac{1}{2}}, h), R^{2g}(\boldsymbol{\theta}_{\frac{1}{2}0}, h), R^{2g}(\boldsymbol{\theta}_{0\frac{1}{2}}, h)\} \in \mathbb{C}^{4\times 16}, \\ P^{3g}(\boldsymbol{\theta}, h) &= \operatorname{diag}\{P^{2g}(\boldsymbol{\theta}_{00}, h), P^{2g}(\boldsymbol{\theta}_{\frac{1}{2}\frac{1}{2}}, h), P^{2g}(\boldsymbol{\theta}_{\frac{1}{2}0}, h), P^{2g}(\boldsymbol{\theta}_{0\frac{1}{2}}, h)\} \in \mathbb{C}^{16\times 4}, \\ (\mathcal{L}^{3g}(\boldsymbol{\theta}, h))^{-1} &= (I^{2g} - (M^{2g}(2\boldsymbol{\theta}, 2h))^{\gamma}) \\ &\quad (\operatorname{diag}\{\mathcal{L}^{2g}(\boldsymbol{\theta}_{00}, h), \mathcal{L}^{2g}(\boldsymbol{\theta}_{\frac{1}{2}\frac{1}{2}}, h), \mathcal{L}^{2g}(\boldsymbol{\theta}_{\frac{1}{2}0}, h), \mathcal{L}^{2g}(\boldsymbol{\theta}_{0\frac{1}{2}}, h)\})^{-1} \in \mathbb{C}^{4\times 4} . \end{aligned} \tag{2.17}$$

Of course, $M^{2g}(2\boldsymbol{\theta}, 2h)$ can be calculated using $S^{2g}(\boldsymbol{\theta}, h)$ and (2.8) if we replace h by $2h$ and $\boldsymbol{\theta}$ by $2\boldsymbol{\theta}$.

Analogous to the two-grid factor $\rho_{2g}(h)$ from (2.9), we obtain the three-grid convergence factor as the supremum of the spectral radii from certain block-matrices:

$$\rho_{3g}(h) := \sup_{\boldsymbol{\theta}\in\tilde{\Theta}_{3g}} \rho(M^{3g}(\boldsymbol{\theta},h)). \tag{2.18}$$

The considerations from Remark 1 concerning the boundedness of $\rho_{2g}(h)$ carry over to the three-grid factors calculated in section 3.

Remark 2 (generalization to d dimensions, k grids, and systems of equations). In the most general case, we consider a d-dimensional problem and apply k-grid cycles to a system of q equations. Then, every low-frequency $\boldsymbol{\theta} \in \Theta_{kg} := (-2^{1-k}\pi, 2^{1-k}\pi]^d$ is coupled with $2^{d(k-1)} - 1$ high frequencies. Accordingly, the related $2^{k-1}h$-harmonics are of dimension $2^{d(k-1)}$. Each operator of the k-grid cycle acts on the whole system and the dimensions of the corresponding block-matrices (see (2.8) and (2.17) for the two-dimensional scalar case with two- and three-grid cycles, respectively) are given by

$$I^{kg},\ S^{kg}(\boldsymbol{\theta},h),\ L^{kg}(\boldsymbol{\theta},h) \in \mathbb{C}^{2^{d(k-1)}q\times 2^{d(k-1)}q}, \quad R^{kg}(\boldsymbol{\theta},h) \in \mathbb{C}^{2^{d(k-2)}q\times 2^{d(k-1)}q},$$
$$P^{kg}(\boldsymbol{\theta},h) \in \mathbb{C}^{2^{d(k-1)}q\times 2^{d(k-2)}q}, \quad \mathcal{L}^{kg}(\boldsymbol{\theta},h) \in \mathbb{C}^{2^{d(k-2)}q\times 2^{d(k-2)}q}.$$

The evaluation of k-grid cycles appears to be quite complicated and costly for many-level cycles, but one should take into account that the k-grid operators (2.6) are recursively defined and can be expressed in terms of two-grid operators. This means that the entries of a k-grid Fourier matrix representation are given by certain two-grid Fourier symbols; see (2.17). *In practice, however, it should usually be enough to perform a three-grid analysis to obtain sufficient insight into a multigrid method.*

Remark 3 (finite-dimensional Fourier space). Note that the Fourier space (2.4) has a nondenumerable basis as $\boldsymbol{\theta}$ varies continuously in $(\pi,\pi]^2$. The use of infinite-dimensional spaces and operators leads to some technical simplifications in the analysis; see [20]. However, in general, the suprema from (2.9), (2.10), and (2.18) cannot be calculated analytically. Therefore, we restrict our practical computations in section 3 to a finite-dimensional Fourier space which is related to the mesh size h under consideration:

$$\mathcal{F}_{finite} := \operatorname{span}\{e^{i\boldsymbol{j}\boldsymbol{\theta}} : \boldsymbol{\theta} \in \Theta_{finite} := (-\pi,\pi]^2 \cap G_{h_{\boldsymbol{\theta}}}\}$$
$$\text{with } G_{h_{\boldsymbol{\theta}}} := \{\boldsymbol{\theta} = h_{\boldsymbol{\theta}}\boldsymbol{j} = (h_{\boldsymbol{\theta}}j_x, h_{\boldsymbol{\theta}}j_y) \text{ with } h_{\boldsymbol{\theta}} = 2\pi h\,, \boldsymbol{j} \in \mathbb{Z}^2\}\,.$$

The definitions of $\tilde{\Theta}_{2g}$, $\tilde{\Theta}_{3g}$, $\mathcal{F}^{2g}$, and $\mathcal{F}^{3g}$ have to be changed accordingly. Hence the suprema are replaced by maxima, which can easily be calculated numerically. Using this finite-dimensional Fourier space, the infinite Fourier analysis becomes an exact analysis for certain model problems on rectangular domains with periodic boundary conditions. Pure periodic boundary conditions lead to a singular boundary value problem in general. This necessitates a compatibility condition for every iterative solution method, which directly corresponds to the exclusion of the "zero" frequency in the analysis; see Remark 1. More details can be found, for example, in [20, 21].

2.4. Generalization for multigrid as a preconditioner for GMRES(m). In this section, we briefly describe the generalization of the above analysis to multigrid as a right preconditioner for GMRES(m). For a detailed discussion with respect to the two-grid analysis, we refer to [24].

As Krylov subspace methods are commonly described using matrix and vector notation, we consider the linear system $Lu = f$, related to (2.1) with $n = k$. A three-grid (or, more generally, a multigrid) cycle can be described by the matrix splitting, $Cu_j + (L - C)u_{j-1} = f$, where u_j and u_{j-1} represent a new and a previous approximation. This formulation is equivalent to

$$u_j = u_{j-1} + C^{-1}(f - Lu_{j-1}) \quad \text{and} \quad r_j = (I - LC^{-1})r_{j-1}$$

with the residual vectors r_j, r_{j-1} and the residual transformation matrix

$$I - LC^{-1} = LML^{-1}, \tag{2.19}$$

where M denotes the three-grid iteration matrix. GMRES(m) searches for a new approximation u_j with corresponding residual r_j in the Krylov subspace

$$K^m(LC^{-1}, r_{j-m}) := \text{span}[r_{j-m}, (LC^{-1})r_{j-m}, \dots, (LC^{-1})^{m-1}r_{j-m}] .$$

It selects the new solution by minimizing the residual in the discrete Euclidean 2-norm

$$||r_j||_2 = \min\{||P_m(LC^{-1})r_{j-m}||_2 \ \mid \ P_m \in \Pi_m\}, \tag{2.20}$$

where Π_m denotes the set of all polynomials of degree at most m with $P_m(0) = 1$. For convenience, $j \geq m$ is assumed. Since we are interested in the asymptotic convergence of multigrid preconditioned GMRES with a restart after m iterations, we focus on the residuals $r_m, r_{2m}, \dots, r_{i\cdot m}$. Then a "complete" iteration with iteration index i consists of m multigrid preconditioned GMRES(m) steps. The GMRES(m)-polynomial which characterizes the ith complete iteration is denoted by P_m^i, leading to the following recursion for the corresponding residual:

$$r_{i\cdot m} = P_m^i(LC^{-1})r_{(i-1)\cdot m}. \tag{2.21}$$

As unitary transformations do not affect the convergence properties of GMRES, we consider the Fourier representations $\widetilde{M}^{3g}$ and $\widetilde{L}^{3g}$ instead of the representations M and L with respect to the Euclidean basis. More precisely, we use the finite-dimensional variants

$$\widetilde{M}^{3g} := [M^{3g}(\boldsymbol{\theta}, h)]_{\boldsymbol{\theta} \in \tilde{\Theta}_{3g} \cap G_{h_{\boldsymbol{\theta}}}} \quad \text{and} \quad \widetilde{L}^{3g} := [L^{3g}(\boldsymbol{\theta}, h)]_{\boldsymbol{\theta} \in \tilde{\Theta}_{3g} \cap G_{h_{\boldsymbol{\theta}}}}$$

to allow an explicit calculation; see Remark 3. Assuming a repeated application of preconditioned GMRES(m), the following function g has to be minimized in order to find the coefficients α_k^i ($k = 1, ..., m$) of the ith GMRES(m)-polynomial P_m^i (see (2.19), (2.20), and (2.21)):

$$g(\alpha_1^i, \dots, \alpha_m^i) := (P_m^i(I - \widetilde{L}^{3g}\widetilde{M}^{3g}(\widetilde{L}^{3g})^{-1})\tilde{r}_{(i-1)m}, P_m^i(I - \widetilde{L}^{3g}\widetilde{M}^{3g}(\widetilde{L}^{3g})^{-1})\tilde{r}_{(i-1)m}).$$

The α_k^i are obtained by solving the linear system

$$\begin{aligned} \frac{\partial g}{\partial \alpha_\ell^i} &= 2\sum_{k=1}^{m} \alpha_k^i((I - \widetilde{L}^{3g}\widetilde{M}^{3g}(\widetilde{L}^{3g})^{-1})^\ell \tilde{r}_{(i-1)m}, (I - \widetilde{L}^{3g}\widetilde{M}^{3g}(\widetilde{L}^{3g})^{-1})^k \tilde{r}_{(i-1)m}) \\ &\quad + 2((I - \widetilde{L}^{3g}\widetilde{M}^{3g}(\widetilde{L}^{3g})^{-1})^\ell \tilde{r}_{(i-1)m}, \tilde{r}_{(i-1)m}) = 0 \qquad \text{for } \ell = 1, \dots, m. \end{aligned} \tag{2.22}$$

The solution of (2.22) can easily be computed for every iteration index i due to the sparse block structure of $(I - \widetilde{L}^{3g}\widetilde{M}^{3g}(\widetilde{L}^{3g})^{-1})^\ell$ ($\ell = 1, \dots, m$) if the previous

Fourier transformed residual $\tilde{r}_{(i-1)m}$ is given. We simply prescribe a randomly chosen initial residual $\tilde{r}_0$. This allows the calculation of $\alpha_\ell^1 (\ell = 1, \dots, m)$ by (2.22) and gives $\tilde{r}_{1\cdot m} = P_m^1 (I - \widetilde{L}^{3g} \widetilde{M}^{3g} (\widetilde{L}^{3g})^{-1}) \tilde{r}_0$. Then the computation of $\tilde{r}_{i\cdot m}$ for $i > 1$ is straightforward due to its recursive definition; see (2.21). This leads to an average reduction factor $\rho_{3g}^{acc}(i,m)$ for a complete iteration, which can be obtained by the three-grid Fourier analysis

$$\rho_{3g}^{acc}(i,m) := \left[\left(\frac{||\tilde{r}_{i\cdot m}||_2}{||\tilde{r}_0||_2} \right)^{1/m} \right]^{1/i}. \tag{2.23}$$

The superscript "acc" is used as an abbreviation for "accelerated," since the combination of multigrid and GMRES(m) can be interpreted as an acceleration of the multigrid convergence speed by an additional application of GMRES(m).

In all tests, presented in section 3, $\rho_{3g}^{acc}(i,m)$ tends to a constant for $i \geq 20$. The particular choice of the initial residual $\tilde{r}_0$ does not influence the average reduction factors for $i \gg 1$, which is confirmed by systematic test calculations. Thus it is expected that $\rho_{3g}^{acc}(m) := \rho_{3g}^{acc}(20,m)$ matches well with numerical reference values.

If we use the above Fourier representation $I - \widetilde{L}^{3g} \widetilde{M}^{3g} (\widetilde{L}^{3g})^{-1}$, the corresponding spectrum can be calculated numerically. The common way (see, for example, [15, 16]) to analyze the convergence of GMRES is to exploit information about the spectrum σ of the iteration matrix LC^{-1}.

Suppose that all eigenvalues of $I - \widetilde{L}^{3g} \widetilde{M}^{3g} (\widetilde{L}^{3g})^{-1}$ are located in an ellipse $E(c,d,a)$ which excludes the origin. $(c,0)$ denotes the center, d denotes the focal distance, and a denotes the major semiaxis. Note that σ is always symmetric with respect to the real axis, so we only consider ellipses which are aligned with the axes and where the ordinate of the center equals zero. Then it is known [16] that the absolute value of the polynomial

$$t_m(z) := T_m\Big(\frac{c}{d} - \frac{1}{d}\, z\Big) \Big/ T_m\Big(\frac{c}{d}\Big) = T_m(\widehat{z}) \Big/ T_m\Big(\frac{c}{d}\Big) \quad \text{with} \quad z, \widehat{z} := \Big(\frac{c}{d} - \frac{1}{d}\, z\Big) \in \mathbb{C}$$

is small on the spectrum of $I - \widetilde{L}^{3g} \widetilde{M}^{3g} (\widetilde{L}^{3g})^{-1}$. Here T_m represents the Chebychev polynomial of degree m of the first kind; see [16]. If $I - \widetilde{L}^{3g} \widetilde{M}^{3g} (\widetilde{L}^{3g})^{-1}$ is diagonalizable, $I - \widetilde{L}^{3g} \widetilde{M}^{3g} (\widetilde{L}^{3g})^{-1} = XDX^{-1}$, then (2.20) yields

$$\begin{aligned} ||\tilde{r}_{i\cdot m}||_2 &\leq ||t_m(I - \widetilde{L}^{3g} \widetilde{M}^{3g} (\widetilde{L}^{3g})^{-1})||_2 \, ||\tilde{r}_{(i-1)m}||_2 \\ &\leq [||t_m(I - \widetilde{L}^{3g} \widetilde{M}^{3g} (\widetilde{L}^{3g})^{-1})||_2]^i \, ||\tilde{r}_0||_2 \leq \left[\kappa_2(X)\, T_m\Big(\frac{a}{d}\Big) / T_m\Big(\frac{c}{d}\Big) \right]^i ||\tilde{r}_0||_2, \end{aligned}$$

where $\kappa_2(X)$ denotes the spectral condition number of the transformation matrix X [16]. Using these inequalities, we obtain for an arbitrary complete iteration i

$$\rho_{3g}^{acc}(i,m) \quad \leq \quad N_m^E \quad \leq \quad (\kappa_2(X))^{1/m}\, T_m^E \quad \text{with} \tag{2.24}$$

(2.25)

$$N_m^E := (||t_m(I - \widetilde{L}^{3g} \widetilde{M}^{3g} (\widetilde{L}^{3g})^{-1})||_2)^{1/m} \quad \text{and} \quad T_m^E := \left(T_m\Big(\frac{a}{d}\Big) / T_m\Big(\frac{c}{d}\Big) \right)^{1/m}$$

as approximations for the average reduction factors of m multigrid preconditioned GMRES(m) steps (see (2.23)).

Remark 4 (determination of ellipses). There seems to be no simple way to determine the "optimal" ellipse for a given spectrum σ which minimizes T_m^E and N_m^E from (2.25). Thus it is proposed in [8] to compute a rectangle containing the spectrum σ and then to calculate the ellipse of smallest area which encloses this rectangle. Both steps of this two-stage strategy are rather simple and straightforward (see [8]), but the resulting ellipses may cover much too large an area due to the first "auxiliary" step. The resulting estimates reflect the qualitative convergence behavior of GMRES(m), but the explicit values are far too pessimistic in general. Therefore, we tune the ellipses by hand. It is well known that each ellipse is uniquely defined if we prescribe three points that should lie on the ellipse. As a first guess, we select those three eigenvalues contained in σ with maximal real part (λ_{max}^{Re}), with minimal real part (λ_{min}^{Re}), and with maximal imaginary part (λ_{max}^{Im}). Then the semiaxis in the x-direction a_x, the semiaxis in the y-direction a_y, and the center $(c, 0)$ of the ellipse are given by

$$a_x = \frac{\mathrm{Re}(\lambda_{max}^{Re}) - \mathrm{Re}(\lambda_{min}^{Re})}{2}, \quad c = \mathrm{Re}(\lambda_{min}^{Re}) + a_x, \quad \text{and} \quad a_y = \frac{\mathrm{Im}(\lambda_{max}^{Im})}{\sqrt{1 - \frac{\mathrm{Re}(\lambda_{max}^{Im}) - c}{a_x^2}}}.$$

$\mathrm{Re}(\lambda)$ and $\mathrm{Im}(\lambda)$ denote the real and imaginary part of the complex eigenvalue λ. (In this way, the ellipse from Figure 3.2b is calculated.) If this first guess does not contain the whole spectrum, the ellipse is carefully enlarged until it covers σ. (An example is given in Figure 3.2a.) Although this strategy might not be very satisfactory from a mathematical viewpoint, it yields sharper estimates which can be easily calculated.

In [17] it is stated that (2.24) is an asymptotic result and that the actual residual norm should rather behave like T_m^E without $\kappa_2(X)$. This presumption, in connection with the two-grid Fourier analysis, is validated in [24], where it is found that the heuristic estimate T_m^E gives a certain insight into the asymptotic accelerated two-grid convergence, whereas the upper bound N_m^E is too pessimistic in general. Therefore, some explicit values for T_m^E based on the spectra of three-grid iteration matrices are given in section 3 and compared with asymptotic numerical convergence results. However, the main focus lies on $\rho_{3g}^{acc}(m)$.

3. Applications of three-grid Fourier analysis. In order to demonstrate the benefits of the three-grid analysis, we consider several equations, discretizations, and multigrid components. The applications range from the nicely elliptic Poisson equation in connection with standard components to singular perturbation problems with more advanced multigrid components. By considering a large number of smoothers and transfer operators, we intend to show the large range of applicability of the three-grid analysis. In each of the following three subsections, we consider coarse grid correction problems which can often be solved by algebraic multigrid (AMG) [19], because AMG implicitly selects the "correct" coarsening strategy for the problem under consideration, or by a special relaxation method. Of course, it is possible to adapt the Fourier analysis from section 2 to nonstandard coarsenings or to sophisticated smoothers. However, we try to keep the multigrid method simple and search for possible improvements by carefully chosen transfer operators and Galerkin coarse grid discretizations. Furthermore, we investigate the use of an additional acceleration with GMRES(m) of nonoptimal but easy-to-program multigrid methods. The main purpose is to evaluate the additional insights coming from the three-grid Fourier analysis.

The theoretical estimates are compared with numerical experiments whose convergence is indicated by $\rho_n(k\mathrm{g})$, which denotes the average defect reduction after 100

TABLE 3.1
MG1 applied to the Poisson equation, $h = 1/128$.

Cycle	$\rho_{1g}(h)$	$\rho_{2g}(h)$	$\rho_{3g}(h)$	ρ_n(3g)	ρ_n(7g)
V(1,1)	0.063	0.074	0.106	0.105	0.119
V(2,0)	0.063	0.074	0.133	0.132	0.170
V(0,2)	0.063	0.074	0.140	0.138	0.179
W(1,1), W(2,0), W(0,2)	0.063	0.074	0.074	0.073	0.073

iterations for the corresponding solution method involving k grids. We choose such a large number of iterations because the theoretical values $\rho_{2g}(h)$ and $\rho_{3g}(h)$ refer to asymptotic convergence factors. For nonsymmetric problems like the convection-dominated examples from section 3.3, it might take a large number of iterations before the asymptotic behavior is observed. An alternative is to consider norms of the three-grid operator, like the defect reduction norm

(3.1)
$$\sigma_{3g}(h) := \sup_{\boldsymbol{\theta}\in\tilde{\Theta}_{3g}} \sqrt{\rho(L^{3g}(\boldsymbol{\theta},h)M^{3g}(\boldsymbol{\theta},h)(L^{3g}(\boldsymbol{\theta},h))^{-1}(L^{3g}(\boldsymbol{\theta},h)M^{3g}(\boldsymbol{\theta},h)(L^{3g}(\boldsymbol{\theta},h))^{-1})^*)},$$

which can be obtained straightforwardly by the above analysis. The star * in (3.1) denotes, as usual, the adjoint of the matrix.

3.1. Poisson equation. The first example deals with the well-known 5-point discretization of the Poisson equation,

$$-\Delta u(\boldsymbol{x}) = 1 \quad \text{on } \Omega = (0,1)^2, \qquad u(\boldsymbol{x}) = 0 \quad \text{on } \Gamma = [0,1]^2 \setminus \Omega. \tag{3.2}$$

An efficient multigrid method [20] for this problem, denoted by $MG1$, consists of

- direct $2h$-, $4h$-, etc. coarse grid discretizations,
- bilinear interpolation of coarse grid corrections and full weighting of residuals, and
- red-black Gauss–Seidel relaxation.

Table 3.1 compares the analytical predictions from the one-, two-, and three-grid analysis with numerical reference values ρ_n(3g) and ρ_n(7g) for several 3- and 7-grid cycles. This table illustrates that even for such a simple and well-understood problem there is a difference between the performance of a V-cycle and a W-cycle and pre- and postsmoothing which cannot be displayed by Fourier two-grid analysis, whereas the different behavior of the cycle variants is very accurately predicted by the three-grid estimates $\rho_{3g}(h)$.

Remark 5 (maintaining the two-grid convergence). As it is seen in Table 3.1, one has to choose the multigrid W-cycle to obtain the two-grid convergence factor. This is indicated by the Fourier analysis. The theoretical predictions for the two- and three-grid factors are equal only for the W-cycle. If we replace the 5-point discretizations on the coarse grids by operators based on Galerkin coarsening with full weighting and bilinear interpolation, the V-cycle also leads to k-independent fast convergence. Using a four-color Gauss–Seidel relaxation for the resulting symmetric 9-point operators, we get for a V(1,1)-cycle $\rho_{1g}(h) = \rho_{2g}(h) = \rho_{3g}(h) = 0.063$. This value is validated by the corresponding numerical calculation for a 7-grid method.

A second multigrid variant, $MG2$ [1], with a simplified coarse grid correction is given by

TABLE 3.2
*MG*2 [1] *applied to the Poisson equation,* $h = 1/128$.

V(1,1)			W(1,1)		
$\rho_{1g}(h)$	$\rho_{2g}(h)$	$\rho_{3g}(h)$	$\rho_{1g}(h)$	$\rho_{2g}(h)$	$\rho_{3g}(h)$
0.06	0.50	0.75	0.06	0.50	0.62

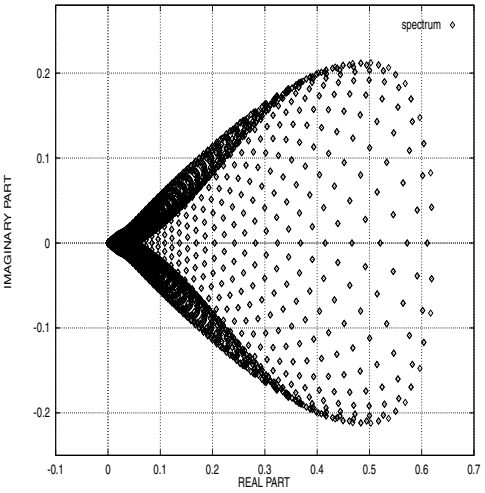

FIG. 3.1a. $\alpha = 1$

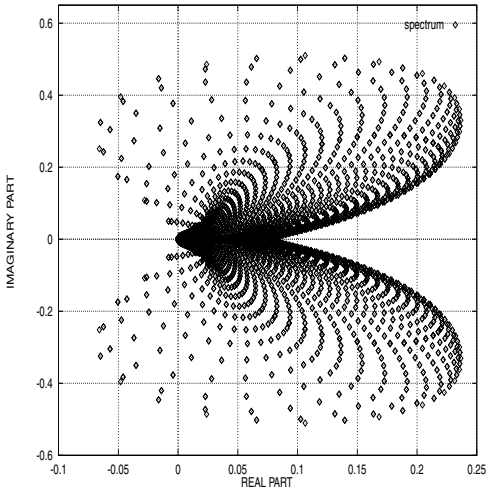

FIG. 3.1b. $\alpha = 2$

FIG. 3.1. *Eigenvalue spectra from Fourier analysis for three-grid* $W(1,1)$*-cycles of MG*2 [1] *with and without rescaling applied to the Poisson equation,* $h = 1/128$.

- Galerkin coarse grid discretizations,
- piecewise constant interpolation and its transpose as transfer operators, and
- symmetric lexicographical Gauss–Seidel relaxation.

Modified versions of this strategy are used in the so-called aggregation-type AMG approaches, which might be useful for problems on unstructured grids; see, for example, [1, 22]. A direct application of this method to the Poisson equation leads to inefficient and strongly h-dependent V- (and W-) cycles. It can be easily shown that each of the coarse grid operators is off by a factor of 2 compared to the discretization on the next finer grid [1, 19]. A simple recursive argument yields that the V-cycle convergence on k grids is limited by $\rho_{kg}(h) \geq 1 - 2^{-k+1}$ ($\rho_{2g}(h) \geq 0.5$, $\rho_{3g}(h) \geq 0.75, \dots$) [19]. Table 3.2 shows that these limiting values can be confirmed by Fourier two- and three-grid analysis.

The above considerations motivate us to rescale the coarse grid Galerkin operators by $1/\alpha$ with α close to 2, $L_{n-1} = 1/\alpha\, \check{R}_n^{n-1} L_n \check{P}_{n-1}^n$, as it is proposed in [1]. For $\alpha = 2$, the Galerkin operators coincide with the standard 5-point discretizations on all grids. Figure 3.1 demonstrates the strong influence of this rescaling on the eigenvalue distribution of a W(1,1) three-grid cycle from Fourier analysis.

Comparing Tables 3.2 and 3.3, one observes the improvement of the two- and three-grid factors due to the rescaling. However, the coarse grid correction problem is not completely solved for V-cycles which can be deduced from the big differences between the one-, two-, and three-grid estimates and which is validated by the further increasing numerical reference value $\rho_n(7\text{g})$ for a 7-grid cycle. This behavior might refer to the fact that the order of the transfer operators (see, for example, [10, 12, 23])

TABLE 3.3
MG2 [1] with a rescaling by $\alpha = 2$ applied to the Poisson equation, $h = 1/128$.

	$MG2$ as a solver				
Cycle	$\rho_{1g}(h)$	$\rho_{2g}(h)$	$\rho_{3g}(h)$	ρ_n(3g)	ρ_n(7g)
V(1,1)	0.06	0.44	0.68	0.66	0.82
W(1,1)	0.06	0.44	0.52	0.50	0.51

	$MG2$ as a preconditioner, $m = 5$		
Cycle	$\rho_{3g}^{acc}(m)$	ρ_n(3g)	ρ_n(7g)
V(1,1)	0.44	0.42	0.53
W(1,1)	0.36	0.34	0.35

in the multigrid process is too low compared to the order of the partial differential equation.

By combining $MG2$ with GMRES(m), one finds satisfactory convergence factors with a rather small Krylov subspace. The actual improvement for a three-grid method can be accurately predicted by $\rho_{3g}^{acc}(m)$; see Table 3.3.

Remark 6 (acceleration on coarse grids, F-cycle convergence). As the coarse grid difficulty occurs on all coarser grids, it seems reasonable to incorporate the Krylov acceleration into the multigrid cycle, like in [14], or to apply it *only on the coarse grids*. In the present example, one obtains ρ_n(7g)=0.52 for a V(1,1)-cycle if GMRES($m = 5$) is applied only on the coarse grids. In this way, it is possible to reduce the storage because on coarser grids much less storage is needed for a Krylov subspace. Furthermore, the multigrid F-cycle yields very similar convergence factors as the W-cycle, both as a solver and as a preconditioner.

Of course, these simple transfer operators are not at all an optimal choice for problem (3.2), especially compared to $MG1$ (see Table 3.1) or to AMG [19]. But it is a first example of a multigrid method with a coarse grid correction difficulty already for the Poisson equation and therefore an illustrative starting example. Furthermore, the method is easy to program and can be seen as a basis for more advanced aggregation-type AMG methods.

3.2. Rotated anisotropic diffusion equation. Next we discuss the standard 9-point discretization (see, for example, [23]) of the rotated anisotropic diffusion equation

$$-(c^2 + \varepsilon s^2)\, u_{xx}(\boldsymbol{x}) - 2(\varepsilon - 1)cs\, u_{xy}(\boldsymbol{x}) - (\varepsilon c^2 + s^2)\, u_{yy}(\boldsymbol{x}) = 1 \quad \text{on } \Omega = (0,1)^2$$
$$\text{with} \quad c = \cos(\beta),\ s = \sin(\beta), \quad u(\boldsymbol{x}) = 0 \quad \text{on } \Gamma = [0,1]^2 \setminus \Omega.$$

This differential operator corresponds to $-u_{\xi\xi} - \varepsilon u_{\eta\eta}$ in a (ξ, η)-coordinate system which can be obtained by rotating the (x, y)-system by an angle of β [23]. We set $\beta = 45°$. For $\varepsilon \to 0$ this equation is no longer elliptic. Using standard grid coarsening and Gauss–Seidel smoothing, this leads to coarse grid correction difficulties which limit the two-grid convergence to a factor of 0.75; see, for instance, [24]. The same recursive argument as in the previous subsection yields a lower bound for the V-cycle convergence on k grids which is given by $\rho_{kg}(h) \geq 1 - 4^{-k+1}$ ($\rho_{2g}(h) \geq 0.75$, $\rho_{3g}(h) \geq 0.9375, \dots$). These bounds can be established by Fourier two- and three-grid analysis as can be seen from Table 3.4, where $MG1$ is applied to the rotated anisotropic diffusion equation. Switching to a W-cycle leads to a slight improvement, which is well predicted by the three-grid analysis.

If $MG1$ is used as a preconditioner, it is possible to obtain an acceptable W-cycle

TABLE 3.4
$MG1$ applied to the rotated anisotropic diffusion equation, $\beta = 45°, \varepsilon = 10^{-5}$, $h = 1/128$.

	$MG1$ as a solver				
Cycle	$\rho_{1g}(h)$	$\rho_{2g}(h)$	$\rho_{3g}(h)$	ρ_n(3g)	ρ_n(7g)
V(1,1)	0.35	0.76	0.94	0.92	0.95
W(1,1)	0.35	0.76	0.90	0.87	0.89

	$MG1$ as a preconditioner, $m = 5$			
Cycle	T_m^E	$\rho_{3g}^{acc}(m)$	ρ_n(3g)	ρ_n(7g)
V(1,1)	0.79	0.68	0.63	0.73
W(1,1)	0.67	0.58	0.52	0.55

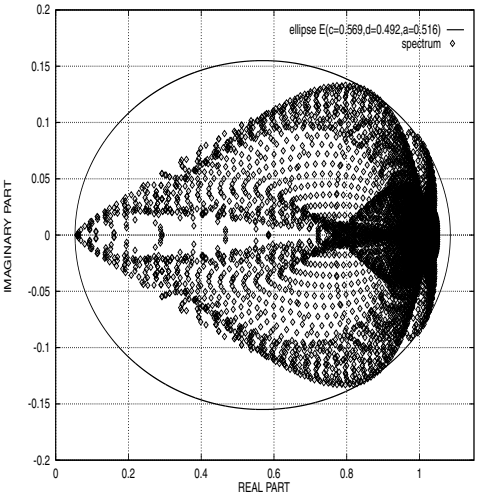

FIG. 3.2a. $MG1$

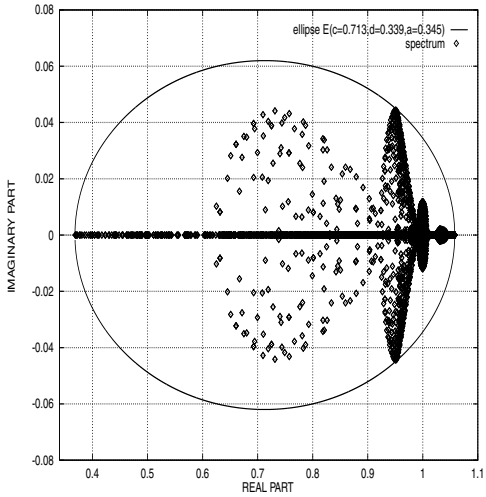

FIG. 3.2b. $MG3$

FIG. 3.2. *Eigenvalue spectra of $I - \widetilde{L}^{3g}\widetilde{M}^{3g}(\widetilde{L}^{3g})^{-1}$ for three-grid $V(1,1)$-cycles of $MG1$ and $MG3$ applied to the rotated anisotropic diffusion equation, $\beta = 45°, \varepsilon = 10^{-5}$, $h = 1/128$.*

convergence, whereas the V-cycle convergence for a 7-grid method remains unsatisfactory. Again, the analytical values $\rho_{3g}^{acc}(m)$ yield reliable predictions that are more accurate than those indicated by T_m^E. As an example, Figure 3.2a shows the $V(1,1)$-cycle spectrum of $I - \widetilde{L}^{3g}\widetilde{M}^{3g}(\widetilde{L}^{3g})^{-1}$ from Fourier analysis for $MG1$ and the corresponding ellipse which is used to calculate T_m^E. For a more detailed discussion of such values and spectra, see [24], as the main focus in this paper lies on the three-grid analysis.

In the context of Galerkin coarsening for the rotated anisotropic diffusion equation, it is interesting to investigate the multigrid method, $MG3$,

- Galerkin coarse grid discretizations,
- matrix-dependent prolongation and restriction by de Zeeuw [27], and
- four-color Gauss–Seidel relaxation.

Comparing Tables 3.4 and 3.5, we see a remarkable improvement of the two-grid convergence factor. For this example, however, Fourier one- and two-grid analysis yield somewhat misleading results. At first sight, the coarse grid correction problem seems to be solved since the two-grid value nearly recovers the smoothing factor. But if we look at the increased three-grid values, one has to expect that the multigrid convergence deteriorates further, which is validated by the numerical reference values

TABLE 3.5
MG3 applied to the rotated anisotropic diffusion equation, $\beta = 45°, \varepsilon = 10^{-5}$, $h = 1/128$.

	$MG3$ as a solver				
Cycle	$\rho_{1g}(h)$	$\rho_{2g}(h)$	$\rho_{3g}(h)$	$\rho_n(3g)$	$\rho_n(7g)$
$V(1,1)$	0.28	0.36	0.63	0.61	0.87
$W(1,1)$	0.28	0.36	0.47	0.48	0.61

	$MG3$ as a preconditioner, $m = 5$			
Cycle	T_m^E	$\rho_{3g}^{acc}(m)$	$\rho_n(3g)$	$\rho_n(7g)$
$V(1,1)$	0.31	0.29	0.28	0.55
$W(1,1)$	0.21	0.19	0.19	0.27

for the related 7-grid iterations.

On the other hand, we see that the three-grid methods can be nicely accelerated by GMRES(m) with a small Krylov subspace. Thus it can be expected also that the corresponding multigrid iterations are appropriate preconditioners, which is confirmed by the numerical values. The actual performance of the accelerated three-grid methods is very accurately estimated by $\rho_3^{acc}(m)$ and T_m^E. The $V(1,1)$-cycle spectrum of $I - \widetilde{L}^{3g}\widetilde{M}^{3g}(\widetilde{L}^{3g})^{-1}$ from Fourier analysis for $MG3$ and the related ellipse are pictured in Figure 3.2b.

Remark 7 (other Galerkin coarsenings). If the prolongation and restriction from [27] in $MG3$ are replaced by the transfer operators from the nonsymmetric blackbox multigrid by Dendy [7], we find very similar results. These transfer operators are investigated in the next subsection. The application of $MG2$ to this problem cannot be recommended. $MG2$ is mainly developed for elliptic problems and does not converge well for the rotated anisotropic diffusion equation.

Finally, we would like to mention that there are other multigrid components like ILU-type smoothers or nonstandard coarsening to overcome the coarse grid correction difficulty efficiently. De Zeeuw [27], for example, combines his matrix-dependent Galerkin coarsening with a powerful smoother, the incomplete line LU decomposition (ILLU), and obtains very fast multigrid convergence. These improvements might be verified by a straightforward adaption of the presented three-grid analysis.

3.3. Convection diffusion equation. As a third example, we discuss the convection diffusion equation with dominant convection in some detail. Here, it is important to distinguish between *entering* flows with an inflow and outflow boundary and *recirculating* flows for which no real inflow and outflow boundary exist and where the boundary information is mainly diffusing into the domain. In principle, efficient multigrid iterations can be constructed for upstream discretizations if relaxation methods are used with a downstream ordering of grid points. Then the relaxation acts not only as a smoother but also partly as a solver and takes care of problematic characteristic low-frequency error components; see [5]. For entering flows such smoothers can be found among standard relaxation methods, whereas for recirculating flows it is very difficult to construct a smoother with the desired property. Channel-type flows employing higher order upwind discretizations are treated successfully in [13].

For convection-dominated rotating flow problems like

$$-\varepsilon\Delta u(\boldsymbol{x}) + a(x,y)\,u_x(\boldsymbol{x}) + b(x,y)\,u_y(\boldsymbol{x}) = 1 \quad \text{on } \Omega = (0,1)^2 \tag{3.3}$$

$$\text{with} \quad \varepsilon = 10^{-5}, \quad a(x,y) = -\sin(\pi x)\cos(\pi y), \quad \text{and} \quad b(x,y) = \sin(\pi y)\cos(\pi x)\,,$$

$$u(\boldsymbol{x}) = \sin(\pi x) + \sin(13\pi x) + \sin(\pi y) + \sin(13\pi y) \quad \text{on } \Gamma = [0,1]^2 \setminus \Omega,$$

the situation changes if standard smoothers are used, and we observe a similar coarse grid correction difficulty as in the previous subsection. If the direct $2h$-, $4h$-, etc. discretizations are applied on the coarser grids combined with standard coarsening, the two-grid convergence is limited by the factor

$$\rho_{2g}(h) \geq 1 - 2^{-p}, \tag{3.4}$$

where p denotes the order of the discretization [6]. This results in a deterioration of the V-cycle multigrid convergence on k grids given by $\rho_{kg}(h) \geq 1 - 2^{-(k-1)\cdot p}$; see above.

Remark 8 (reliability of the Fourier analysis). Dirichlet boundary effects are neglected by the Fourier analysis as it is presented in this paper. For entering flows, high-frequency boundary data may propagate far into the domain, and thus it should be taken into account by a reliable analysis. This is done by the so-called *half-space* full multigrid (FMG) analysis in [5]. For recirculating flows, however, the influence of the domain boundary is negligible in the limit of small mesh size, and the (*infinite-space*) Fourier analysis is again useful [6].

Remark 9 (Fourier analysis for operators with variable coefficients). A direct application of the Fourier analysis is not possible if we deal with operators $L_h(\boldsymbol{x})$ that are characterized by variable coefficients. However, the analysis can be applied to the locally frozen operator at a fixed grid point $\boldsymbol{\xi}$. Replacing the variable $\boldsymbol{x}$ by a constant $\boldsymbol{\xi}$, one obtains an operator $L_h(\boldsymbol{\xi})$ with *constant frozen* coefficients. In [3] it is motivated that the smoothing or two-grid factor for $L_h(\boldsymbol{x})$ can be bounded by the suprenum over the smoothing or two-grid factors for the locally frozen operators. Thus one may define the following convergence factors in the case of variable coefficients:

$$\rho_{kg}\left(h, L_h(\boldsymbol{x})\right) := \sup_{\boldsymbol{\xi}\in\Omega} \rho_{kg}\left(h, L_h(\boldsymbol{\xi})\right) \quad \text{for} \quad k = 1, 2, 3. \tag{3.5}$$

This means for (3.3) that one has to investigate the whole range of convection angles that occur in the problem. For an explicit calculation, we approximate (3.5) by a repeated application of the Fourier analysis to discretizations of $-\varepsilon\Delta u + a\,u_x + b\,u_y$ with fixed $a = \cos\beta$ and $b = \sin\beta$ for multiples of 3° until the range of possible convection angles $\beta \in [0^\circ, 360^\circ]$ is passed through, as is proposed in [23]. Then, the maximal values for $\rho_{1g}(h,\beta)$, $\rho_{2g}(h,\beta)$, $\rho_{3g}(h,\beta)$, and $\sigma_{3g}(h,\beta)$ are assumed to be upper bounds for problem (3.3).

In this section, we do not consider the acceleration by GMRES(m) in the Fourier analysis. For problems with varying coefficients the analysis from section 2.4 can be adapted in the same way as it is explained in Remark 9, but it has to be interpreted with care, as it has a more qualitative character. In the numerical experiments, however, we often observe a considerable improvement, especially for rotating flow problems.

3.3.1. First order discretization. A first order upwind discretization of (3.3) is given by the following stencil:

$$\frac{\varepsilon}{h^2}\begin{bmatrix} & -1 & \\ -1 & 4 & -1 \\ & -1 & \end{bmatrix} + \frac{1}{2h}\begin{bmatrix} -a-|a| & 2|a| & a-|a| \end{bmatrix} + \frac{1}{2h}\begin{bmatrix} b-|b| \\ 2|b| \\ -b-|b| \end{bmatrix}. \tag{3.6}$$

This discretization is studied in many papers, for instance, in [5, 14, 19, 26], where the coarse grid correction difficulty for geometric multigrid with direct coarse grid

TABLE 3.6
MG4 applied to the convection diffusion equation discretized by a first order upwind scheme, $\varepsilon = 10^{-5}$, $h = 1/256$.

Cycle	$\rho_{1g}(h,\beta)$	$\rho_{2g}(h,\beta)$	$\rho_{3g}(h,\beta)$	$\sigma_{3g}(h,\beta)$	ρ_n(8g)
W(1,1)	0.29 ($\beta = 3°$)	0.22 ($\beta = 6°$)	0.22 ($\beta = 6°$)	0.24 ($\beta = 6°$)	0.20
W(2,1)	0.15 ($\beta = 3°$)	0.17 ($\beta = 6°$)	0.18 ($\beta = 6°$)	0.20 ($\beta = 6°$)	0.17

discretizations is overcome by different remedies, like an overweighting of residuals [5], an additional Krylov acceleration [14], an application of AMG [19], or a special higher order choice of coarse grid discretizations [26]. Many of these approaches can be well analyzed by the Fourier three-grid analysis from section 2.

The convergence factors of the multigrid method by de Zeeuw [27] based on matrix-dependent transfer operators gets worse for discretization (3.6) with an increasing number of grids, even with a powerful relaxation like ILLU. This can be confirmed by the Fourier three-grid analysis. It is possible to improve the convergence properties with another Galerkin coarse grid operator applied in $MG4$:

- Galerkin coarse grid discretizations,
- transfer operators from the nonsymmetric blackbox multigrid by Dendy [7], and
- damped ($\omega = 0.7$) alternating zebra line Gauss–Seidel relaxation.

It was already stated in [26] that the application of this Galerkin coarsening should be useful. The symmetric prolongation, based on the symmetric part of the respective discretization operator $1/2(L_n + L_n^*)$, is similar to the well-known matrix-dependent prolongations for jumping coefficients; see, for instance, [10, 23, 27]. The nonsymmetric restriction, however, is defined as the transpose of a prolongation operator that is based on L_n^* leading to an upstream restriction. This is particularly useful because the coarse-grid operators remain upstream as well and tend to a second order compact upstream discretization. This agrees with the observation that the coarse grid operators must become higher order, at least in the cross-stream direction, to provide a good coarse grid approximation; see [26].

Table 3.6 shows the maximal one-, two-, and three-grid factors for $MG4$ with the corresponding convection angles in brackets; see Remark 9. As the two- and three-grid factors are very similar or even equal, it can be expected that the multigrid convergence for discretization (3.6) is close to these estimates, which is confirmed by the numerical reference for an 8-grid method. The maximal norm values $\sigma_{3g}(h,\beta)$ differ only slightly from the corresponding $\rho_{3g}(h,\beta)$, which indicates that the convergence speed for a single iteration is not much larger than the asymptotic convergence factor. Thus, $\rho_{3g}(h,\beta)$ is a "satisfactory" prediction for the multigrid convergence. This is observed in the numerical convergence history. Furthermore, we see that the damped alternating zebra line relaxation which is a robust smoother for the fine grid discretization [23] keeps this property for the Galerkin coarse grid discretizations resulting from the blackbox transfer operators.

3.3.2. Fourth order compact discretization. We continue with the fourth order compact discretization of (3.3) from [9]. With respect to the Fourier analysis, it is convenient to investigate the difference scheme for constant coefficients; see Remark

TABLE 3.7
MG4 is applied to the convection diffusion equation discretized by a compact fourth order scheme [9], $\varepsilon = 10^{-5}$, $h = 1/128$.

Cycle	$\rho_{1g}(h,\beta)$	$\rho_{2g}(h,\beta)$	$\rho_{3g}(h,\beta)$	$\sigma_{3g}(h,\beta)$
W(1,1)	0.53 ($\beta = 6°$)	0.59 ($\beta = 3°$)	0.77 ($\beta = 6°$)	> 20 ($\beta = 45°$)
W(2,2)	0.27 ($\beta = 6°$)	0.54 ($\beta = 9°$)	0.74 ($\beta = 9°$)	0.85 ($\beta = 18°$)

TABLE 3.8
The convection diffusion equation is discretized by a compact fourth order scheme [9] *using Galerkin coarsening based on the restriction from nonsymmetric blackbox multigrid* [7] *and biquintic interpolation, alternating zebra line Gauss–Seidel relaxation* ($\omega = 0.7$), $\varepsilon = 10^{-5}$, $h = 1/128$.

Cycle	$\rho_{1g}(h,\beta)$	$\rho_{2g}(h,\beta)$	$\rho_{3g}(h,\beta)$	$\sigma_{3g}(h,\beta)$
W(1,1)	0.53 ($\beta = 6°$)	0.46 ($\beta = 6°$)	0.60 ($\beta = 9°$)	0.69 ($\beta = 9°$)
W(2,2)	0.27 ($\beta = 6°$)	0.29 ($\beta = 3°$)	0.46 ($\beta = 9°$)	0.53 ($\beta = 9°$)

Cycle	$\rho_{3g}(h,\beta)$	$\sigma_{3g}(h,\beta)$
W(1,1), $\nu_1(2h) = \nu_2(2h) = 3$	0.46 ($\beta = 6°$)	0.50 ($\beta = 6°$)
W(2,2), $\nu_1(2h) = \nu_2(2h) = 4$	0.31 ($\beta = 9°$)	0.35 ($\beta = 9°$)

9, which reads in stencil notation [25]

$$\frac{\varepsilon}{6h^2}\begin{bmatrix}-1 & -4 & -1\\ -4 & 20 & -4\\ -1 & -4 & -1\end{bmatrix} + \frac{1}{12h}\begin{bmatrix}a-b & -4b & -a-b\\ 4a & 0 & -4a\\ a+b & 4b & -a+b\end{bmatrix} + \frac{1}{24\varepsilon}\begin{bmatrix}ab & -2b^2 & -ab\\ -2a^2 & 4a^2+4b^2 & -2a^2\\ -ab & -2b^2 & ab\end{bmatrix}.$$

Here, a two-grid convergence factor of 0.9375 is predicted by (3.4) for the direct coarse grid discretizations. Applying $MG4$ to this discretization, we find a remarkable improvement of the two-grid factor compared to the standard variant, but the coarse grid problem is not really solved, as is indicated by the increase of the two- and three-grid factors compared to the one-grid values; see Table 3.7. This can be explained by considering the orders of the transfer operators in a Galerkin process for singularly perturbed problems [26]. The sum of these orders ($m_r + m_p$, where the subscripts are abbreviations for restriction and prolongation, respectively) should be greater than the order of the differential equation M plus the order of the discretization p, i.e.,

$$m_r + m_p > M + p. \tag{3.7}$$

This requirement is fulfilled for the multigrid method from Table 3.6 for the first order discretization of (3.3) ($m_r = 1, m_p = 2, M = 1, p = 1$) but is violated in Table 3.7 ($m_r = 1, m_p = 2, M = 1, p = 4$). Note that we set $M = 1$ in this situation because of the dominating convection term. It is already indicated by the large value of σ_{3g} for the W(1,1)-cycle from Table 3.7 that this multigrid method has to be handled with care.

We keep the restriction from $MG4$ in order to maintain the upstream properties of the discretizations on the coarser grids (see [7]) but replace the prolongation by biquintic interpolation ($m_p = 6$). Thus, the above rule (3.7) is satisfied, which leads to a considerable improvement of the multigrid method, as is shown in Table 3.8. Regarding the norm values $\sigma_{3g}(h,\beta)$, one obtains a reliable multigrid method. However, although the one- and two-grid factors are similar, the three-grid factors still increase in the upper part of Table 3.8. This is due to a deterioration of the smoothing property on the coarse grids because there we have larger stencils resulting from the very accurate interpolation in the Galerkin process. The three-grid convergence

factors can be improved if we increase the numbers $\nu_1(2h)$ and $\nu_2(2h)$ of pre- and postsmoothing steps on G_{2h}, as is shown in the lower part of Table 3.8. In this way, it is possible to recover the two-grid factors, which indicates that the coarse grid correction difficulty is solved. From section 3.3.1, it can be expected that the analytical estimates match closely with numerical test calculations, and also for the fourth order discretization. Because of the large stencils, however, this multigrid method cannot be recommended for a practical implementation despite its good (regarding the highly accurate discretization) convergence behavior.

4. Conclusions. We have presented Fourier three-grid analysis for multigrid as a solver and as a preconditioner for GMRES(m). Applying this analysis, it is possible to obtain accurate convergence estimates for elliptic operators and to predict the performance of V- and W-cycles or pre- and postsmoothing. For singularly perturbed problems with coarse grid correction difficulties, the three-grid analysis yields additional valuable insight into the nature of the multigrid convergence problem and allows for an investigation of the benefits of possible remedies, for example, based on certain choices of Galerkin coarse grid discretizations. One can verify the qualitative rule concerning the order of the transfer operators in a Galerkin process for singularly perturbed problems from [26] by quantitative asymptotic convergence and norm estimates.

REFERENCES

[1] D. Braess, *Towards algebraic multigrid for elliptic problems of second order*, Computing, 55 (1995), pp. 379–393.
[2] A. Brandt, *Multi-level adaptive solutions to boundary-value problems*, Math. Comp., 31 (1977), pp. 333–390.
[3] A. Brandt, *Rigorous local mode analysis of multigrid*, in Preliminary Proceedings of the 4th Copper Mountain Conference on Multigrid Methods, Copper Mountain, CO, 1989, pp. 55–133.
[4] A. Brandt, *Rigorous quantitative analysis of multigrid,* I. *Constant coefficients two-level cycle with L_2-norm*, SIAM J. Numer. Anal., 31 (1994), pp. 1695–1730.
[5] A. Brandt and I. Yavneh, *On multigrid solution of high-Reynolds incompressible entering flows*, J. Comput. Phys., 101 (1992), pp. 151–164.
[6] A. Brandt and I. Yavneh, *Accelerated multigrid convergence and high-Reynolds recirculating flows*, SIAM J. Sci. Comput., 14 (1993), pp. 607–626.
[7] J. E. Dendy, Jr., *Blackbox multigrid for nonsymmetric problems*, Appl. Math. Comput., 13 (1983), pp. 261–283.
[8] B. Fischer, A. Ramage, D. J. Silvester, and A. J. Wathen, *On parameter choice and iterative convergence for stabilised discretisations of advection-diffusion problems*, Comput. Methods Appl. Mech. Engrg., 179 (1999), pp. 179–195.
[9] M. M. Gupta, R. P. Manohar, and J. W. Stephenson, *A single cell high order scheme for the convection-diffusion equation with variable coefficients*, Internat. J. Numer. Methods Fluids, 4 (1984), pp. 641–651.
[10] W. Hackbusch, *Multi-Grid Methods and Applications*, Springer-Verlag, Berlin, 1985.
[11] P. W. Hemker, *Fourier Analysis of Grid Functions, Prolongations and Restrictions*, Report NW 98, CWI, Amsterdam, 1980.
[12] P. W. Hemker, *On the order of prolongations and restrictions in multigrid procedures*, J. Comput. Appl. Math., 32 (1990), pp. 423–429.
[13] C. W. Oosterlee, F. J. Gaspar, T. Washio, and R. Wienands, *Multigrid line smoothers for higher order upwind discretizations of convection-dominated problems*, J. Comput. Phys., 139 (1998), pp. 274–307.
[14] C. W. Oosterlee and T. Washio, *Krylov subspace acceleration of nonlinear multigrid with application to recirculating flows*, SIAM J. Sci. Comput., 21 (2000), pp. 1670–1690.
[15] Y. Saad and M. H. Schultz, *GMRES: A generalized minimal residual algorithm for solving nonsymmetric linear systems*, SIAM J. Sci. Statist. Comput., 7 (1986), pp. 856–869.
[16] Y. Saad, *Iterative Methods for Sparse Linear Systems*, PWS Publishing, Boston, 1996.

[17] Y. Saad, *Further analysis of minimum residual iterations*, Numer. Linear Algebra Appl., 7 (2000), pp. 67–93.
[18] R. Stevenson, *On the Validity of Local Mode Analysis of Multi-Grid Methods*, Ph.D. thesis, Rijks University, Utrecht, the Netherlands, 1990.
[19] K. Stüben, *Algebraic Multigrid (AMG): An Introduction with Applications*, Tech. report 53, GMD, St. Augustin, Germany, 1999. This report appeared as an appendix in [21].
[20] K. Stüben and U. Trottenberg, *Multigrid methods: Fundamental algorithms, model problem analysis and applications*, in Multigrid Methods, Lecture Notes in Math. 960, W. Hackbusch and U. Trottenberg, eds., Springer-Verlag, Berlin, 1982, pp. 1–176.
[21] U. Trottenberg, C. W. Oosterlee, and A. Schüller, *Multigrid*, Academic Press, New York, 2001.
[22] P. Vanek, J. Mandel, and M. Brezina, *Algebraic Multigrid on Unstructured Meshes*, UCD/CCM Report 34, University of Colorado, Denver, CO, 1994.
[23] P. Wesseling, *An Introduction to Multigrid Methods*, John Wiley, Chichester, UK, 1992.
[24] R. Wienands, C. W. Oosterlee, and T. Washio, *Fourier analysis of GMRES(m) preconditioned by multigrid*, SIAM J. Sci. Comput., 22 (2000), pp. 582–603.
[25] I. Yavneh, *Analysis of a fourth-order compact scheme for convection-diffusion*, J. Comput. Phys., 133 (1997), pp. 361–364.
[26] I. Yavneh, *Coarse-grid correction for nonelliptic and singular perturbation problems*, SIAM J. Sci. Comput., 19 (1998), pp. 1682–1699.
[27] P. M. de Zeeuw, *Matrix-dependent prolongations and restrictions in a blackbox multigrid solver*, J. Comput. Appl. Math., 33 (1990), pp. 1–27.